npj | climate and atmospheric science

www.nature.com/npjclimatsci

ARTICLE OPEN

Check for updates

Weak Hadley cell intensity changes due to compensating effects of tropical and extratropical radiative forcing

Doyeon Kim[1,4], Hanjun Kim[1,4], Sarah M. Kang[1✉], Malte F. Stuecker[2] and Timothy M. Merlis[3]

The Hadley cell response to globally increasing CO_2 concentrations is spatially complex, with an intensified rising branch and weakened descending branch. To better understand these changes, we examine the sensitivity of the Hadley cell to idealized radiative forcing in different latitude bands. The Hadley cell response is, to first order, governed by the latitudinal structure of the forcing. The strengthening of the upward branch is attributed to tropical forcing, whereas the weakening of the descending branch is attributed to extratropical forcing. These direct radiatively-forced Hadley cell responses are amplified by changes in atmospheric eddy heat transport while being partially offset by changes in gross moist stability and ocean heat uptake. The radiative feedbacks further modulate the Hadley cell response by altering the meridional atmospheric energy gradient. The Hadley cell projections under global warming are thus a result of opposing – and thus compensating – effects from tropical and extratropical radiative forcings.

npj Climate and Atmospheric Science (2022)5:61 ; https://doi.org/10.1038/s41612-022-00287-x

INTRODUCTION

The Hadley cell (HC) is the zonal-mean meridional overturning circulation in the tropics, driven by the equator-to-pole gradient in solar insolation. The HC ascending branch entails the regions with the most extreme rainfall, whereas the HC descending branch coincides with the subtropical dry zones. As the HC is critical to determining the large-scale hydrological cycle, understanding how the HC responds to global warming has crucial socio-economic relevance for the future[1–5].

The HC change features a meridionally complex structure with considerable inter-model uncertainty (Fig. 1). It is characterized by an intensification and an equatorward contraction of the rising branch[6–9] and a weakening and a poleward expansion of the descending branch[10–12]. A weakening of the maximum HC strength is found in both hemispheres in the multi-model mean response (Fig. 1a), but is robust only in the Northern Hemisphere[13] (Fig. 1b). Understanding the mechanisms of these latitudinally varying HC responses is key for constraining future rainfall projections[14].

Noting that HC changes are provoked by perturbations to the top-of-atmosphere (TOA) radiative balance[15,16], the contributions to changes in HC strength can be explained by the energetic framework of radiative feedbacks[17,18]. The energetics framework of Ref. [17] implies that the HC strength is proportional to the poleward atmospheric energy transport by the mean circulation in the tropics while being inversely proportional to the gross moist stability (i.e., energy transport efficiency per unit mass flux). The CO_2-forced HC weakening has been attributed to an increase in gross moist stability that requires less HC mass transport for a given unit of atmospheric energy transport, to an increase in eddy heat flux that causes a reduction in the mean component of atmospheric energy transport, and to radiative feedbacks that become more positive at higher latitudes such as those associated with lapse rate and sea ice changes[17]. The projected overall HC weakening is partially offset by anomalous ocean heat uptake, which features anomalous downward surface fluxes into the subpolar oceans and anomalous upward surface fluxes in the tropics[17]. Hence, the HC weakening is more pronounced in atmosphere models coupled to a slab ocean compared to fully coupled climate model configurations[19,20]. The projected HC weakening is also counteracted by the water vapor feedback that enhances the meridional energy gradient[17]. In the meantime, the cloud feedback can either enhance or reduce the meridional energy gradient and contributes most to the inter-model spread in the HC intensity changes[17]. In general, processes that counteract the projected HC weakening are any climate response that heats lower latitudes at the expense of higher latitudes, thereby enhancing the meridional energy gradient. Conversely, a HC weakening results from any climate response that heats higher latitudes at the expense of lower latitudes, thus reducing the meridional energy gradient. For example, a tropical thermal forcing strengthens the HC, while an extratropical thermal forcing weakens the HC[21]. Therefore, the meridional structure of the climate responses under global warming needs to be understood to explain the net HC intensity changes.

The spatial patterns of the radiatively forced climate response were recently examined with the help of an idealized modeling approach with latitudinally varying CO_2 concentrations (as a conduit for prescribing latitudinally varying radiative forcing)[20,22–24]. Previous studies mimic the effect of regional CO_2 perturbations by prescribing thermal forcings at different horizontal and vertical locations. However, the HC response is found to be sensitive to the prescribed forcing structure (Chang 1995; Son and Lee 2005; Buter et al. 2010; Wang et al. 2012), making it difficult to assess the HC response to thermal forcings. Hence, we choose to analyze the model results of Ref. [23], where CO_2 concentrations are directly quadrupled in different latitude regions – the deep tropics (TROP; 7°S–7°N), the off-equatorial-to-midlatitudes (MLAT; 8°S–59°S and 8°N–59°N), and the polar regions (POLAR; 60°S–90°S and 60°N–90°N) (Fig. 2a; see 'Methods').

[1]Department of Urban and Environmental Engineering, UNIST, Ulsan, Korea. [2]Department of Oceanography and International Pacific Research Center, School of Ocean and Earth Science and Technology, University of Hawai'i at Mānoa, Honolulu, HI, USA. [3]Program in Atmospheric and Oceanic Sciences, Princeton University, Princeton, NJ, USA. [4]These authors contributed equally: Doyeon Kim, Hanjun Kim. ✉email: skang@unist.ac.kr

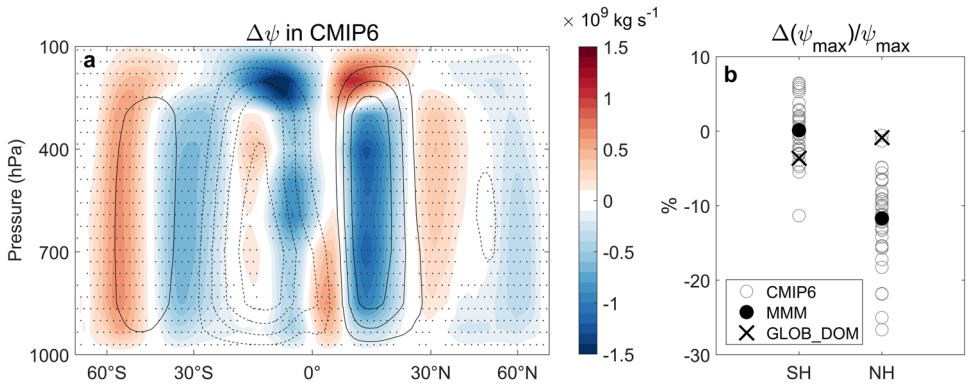

Fig. 1 Hadley circulation responses to global CO_2 forcing in CMIP6. a Multi-model mean changes of the atmospheric annual-mean meridional streamfunction (shading; interval = 10^8 kg s^{-1}) averaged for years 11–60 after an abrupt global quadrupling of CO_2 concentrations from the corresponding pre-industrial control climatology averaged over the last 100 years (contours; interval = 2×10^{10} kg s^{-1}) for 40 CMIP6 models. Positive values (red shading and solid contours) correspond to a clockwise circulation and negative values (blue shading and dashed contours) to a counterclockwise circulation. Stippling indicates areas where at least two third of the models agree on the sign of the change. **b** Percentage changes of the southern and northern Hadley cell intensity ($\Delta\psi_{max}/\psi_{max}$ in %) averaged between 10°-20° latitude in each hemisphere. Each CMIP6 model response is shown with open circles, with the multi-model mean in black closed circles, and the GLOB_DOM experiment response indicated by black crosses.

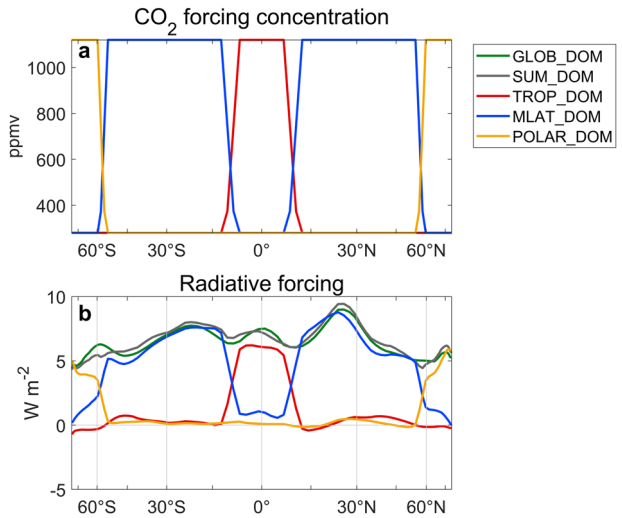

Fig. 2 CO_2 forcing structures and radiative forcings. a The annual- and zonal-mean profile of CO_2 concentration and **b** radiative forcing in GLOB_DOM (green), TROP_DOM (red), MLAT_DOM (blue), POLAR_DOM (yellow), and the sum of all regional forcing experiments SUM_DOM (gray).

We focus on the fully coupled model results that encompass all comprehensive physical processes as well as ocean dynamical effects. The aim of this paper is to elucidate how local and remote radiative forcings distinctively alter the HC strength via different physical processes. Here, we employ comprehensive models with realistic boundary conditions to investigate the HC response to latitudinally varying radiative forcing.

We adopt the previously mentioned energetics framework[17] to quantify the contributions of various feedbacks to the projected HC response. An alternative method for quantifying the HC intensity changes is the feedback locking technique where individual feedbacks of interest (e.g., water vapor, clouds, etc.) are disabled[25–28]. Feedback locking experiments in aqua-planet simulations reveal that the cloud radiative effect dominates the HC weakening in response to increased CO_2 concentration[25,28], a large fraction of which is offset by surface heat exchange response due to surface humidity changes[27]. While the feedback locking technique is useful for quantitatively separating individual effects, it is computationally too expensive for our purpose of disentangling the regional forcing effect in fully coupled model experiments. More importantly, we aim to examine the physical mechanism behind fully coupled models which include all possible interactions between various radiative feedbacks and the ocean circulation changes. Hence, we use the decomposition method, which combines the moist static energy budget, approximate partial radiative perturbation (APRP) method[29], and radiative kernel technique[17], for analyzing the Community Earth System Model version 1.2.2 (CESM1)[30] model results of Ref. [23]. To facilitate understanding of the response in the fully coupled system, the experiments are conducted under three different model configurations with varying degree of ocean coupling (see 'Methods'): an atmospheric general circulation model fully coupled with a dynamic ocean model (DOM), thermodynamically coupled with a slab ocean model (SOM), and with fixed sea surface temperatures (FSST) as boundary conditions.

RESULTS

Hadley cell response to latitudinally varying CO_2 increases

Quadrupling the global CO_2 concentration (i.e., GLOB_DOM) causes an equatorward contraction and a rise of the ascending HC branch[8,20], characterized by the HC strengthening equatorward of 10°S/N and a weakening in the off-equatorial region (Fig. 3a). This is broadly consistent with the response in the Sixth Phase of the Coupled Model Intercomparison Project (CMIP6) models (Fig. 1a) with a pattern correlation coefficient of 0.65 between 40°S and 40°N. However, our CESM1 experiment tends to be an outlier within the CMIP6 ensemble in terms of the hemispheric asymmetry of the HC response. The CMIP multi-model mean response suggests a more robust weakening for the northern HC whereas our GLOB_DOM shows a stronger weakening for the southern HC[31] (Fig. 1b). We emphasize that our aim is not to examine the robust features to global CO_2 increases but to understand the contributions of regional radiative forcings to the HC response, which our analysis suggests is more robust across the models.

In fact, the HC strength changes in GLOB_DOM are barely significant at the 95% confidence level (Fig. 3a). In all model configurations, the HC response to global CO_2 forcing (GLOB; the 1st row in Fig. 3) is well reproduced by the linear sum of the responses to regional CO_2 forcings (SUM; the 2nd row in Fig. 3). This linearity allows us to decompose the HC response in terms of the responses to regional forcings. A relatively weak and insignificant HC response in GLOB_DOM (Fig. 3a) is a result of opposing large

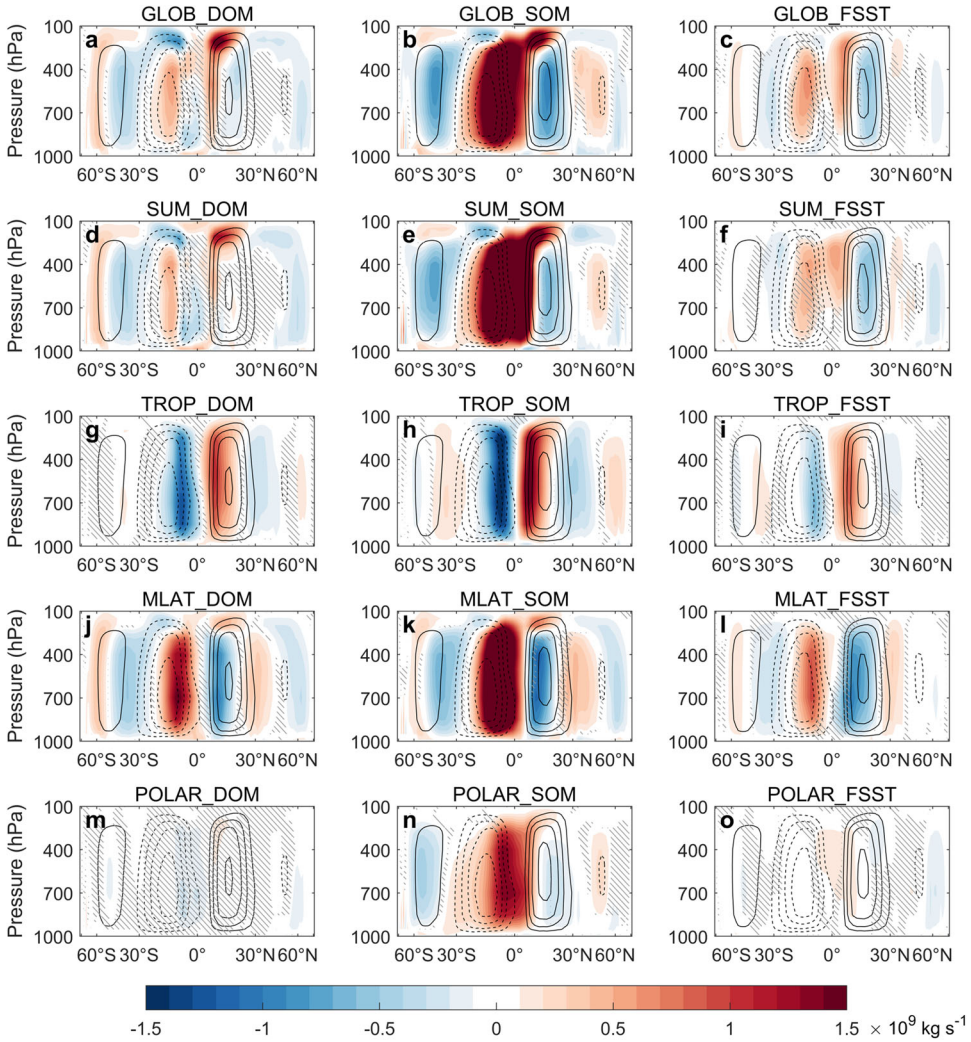

Fig. 3 Hadley circulation responses to different CO_2 forcings in the CESM experiments. The atmospheric annual-mean meridional streamfunction responses in shading (interval = 10^8 kg s^{-1}) relative to the control experiment climatologies shown in contours (interval = 2×10^{10} kg s^{-1}) for **a**–**c** GLOB, **d**–**f** sum of all regional forcing experiments (SUM), **g**–**i** TROP, **j**–**l** MLAT, and **m**–**o** POLAR in the (1st column) DOM, (2nd column) SOM, and (3rd column) FSST configurations. Positive values (red shading and solid contours) correspond to a clockwise circulation and negative values (blue shading and dashed contours) to a counterclockwise circulation. Hatched regions indicate statistically insignificant values at the 95% confidence level based on a two-tailed *t*-test.

responses to regional CO_2 quadrupling forcings in the deep tropics (TROP_DOM; Fig. 3g) and in the off-equatorial-to-midlatitudes (MLAT_DOM; Fig. 3j). The strengthening and narrowing of the HC in TROP_DOM (Fig. 3g) are slightly overcompensated by the weakening and expansion of HC in MLAT_DOM (Fig. 3j). A comparable impact of the TROP and MLAT forcing on the HC response is remarkable given that the global warming response is overwhelmed by MLAT forcing[20] (Supplementary Fig. 1 and Supplementary Fig. 2), highlighting the importance of the spatial structure of climate response rather than the global-mean response for shaping the HC response[25]. The contribution of the polar CO_2 forcing (POLAR; 60°S–90°S and 60°N–90°N) is negligible (Fig. 3m). Hence, POLAR_DOM results are not shown in the subsequent analysis for simplicity. We discuss the consistency of our results in relation to earlier studies in the 'Discussion' section.

Attribution of Hadley cell intensity changes to individual physical processes

To understand the individual physical processes responsible for the dependency of HC intensity changes on CO_2 forcing locations, we attribute the fractional changes in the annual-mean HC strength to the changes in radiative forcing, atmospheric eddy transport, gross moist stability, ocean heat uptake, and TOA radiative feedback (left column of Fig. 4; see 'Methods'). The results are only shown for the DOM configuration. For both hemispheres, positive values indicate a HC strengthening and negative values indicate a HC weakening. Note that individual components are averaged between 10° and 20° latitude in each hemisphere. First, the spatial distribution of CO_2 radiative forcing is the main factor that gives rise to the robust HC strength changes depending on the CO_2 forcing location (Forc in Fig. 4c, e). The TROP forcing increases tropical net energy input by trapping the outgoing longwave radiation, reinforcing the meridional energy gradient (red in Fig. 2b), thereby strengthening the HC (Forc in Fig. 4c). Conversely, the MLAT forcing reduces the meridional energy gradient (blue in Fig. 2b), resulting in a HC weakening (Forc in Fig. 4e). That is, the HC intensity changes to the regional CO_2 forcings are to first order determined by the meridional structures of the radiative forcing, consistent with the expectations of axisymmetric HC theory[32]. The direct effect of increased CO_2 is seen in the FSST experiments, which show that

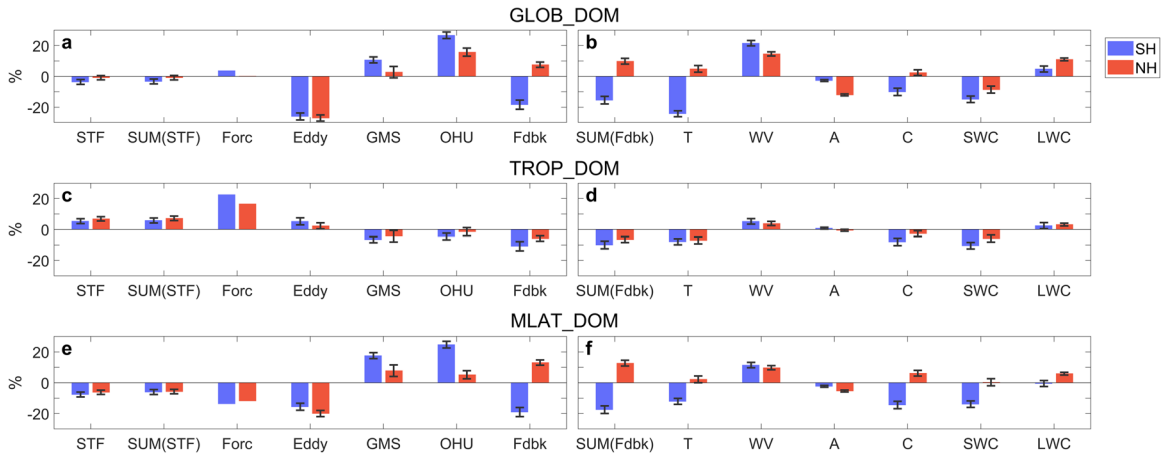

Fig. 4 Decomposition of Hadley circulation intensity responses to different CO_2 forcings. Contributions to changes (unit = %) in the northern (red) and southern (blue) Hadley cell intensity for **a**, **b** GLOB_DOM, **c**, **d** TROP_DOM, and **e**, **f** MLAT_DOM. Fractional changes in Hadley cell intensity (STF), contributions from radiative forcing (Forc), atmospheric eddies (Eddy), gross moist stability (GMS), ocean heat uptake (OHU), and radiative feedback (Fdbk) (see 'Methods'). The summation of all contributions (SUM(STF)) matches well the actual response STF, validating the linear decomposition using Eq. (5). (Right) The Fdbk contributions due to changes in temperature (T), water vapor (WV), surface albedo (A), net cloud feedback (C), and the shortwave (SWC) and longwave (LWC) components of the cloud feedback. The summation of all feedback components (SUM(Fdbk)) matches well with Fdbk, validating the radiative flux decomposition using Eq. (6). Error bars indicate the confidence intervals in which the responses are statistically not different from the control simulation at the 95% confidence level based on a two-tailed *t*-test.

the HC responses are largely consistent with those in the DOM configuration despite the absence of SST changes (compare the 1st and 3rd columns in Fig. 3). The importance of the CO_2 direct effect on the HC has been discussed in previous studies[14,18]. The direct CO_2-forced fraction explains 50% and 75% of the HC intensity responses to TROP and MLAT forcing, respectively, based on the fractional changes in the HC intensity (Fig. 3i, l vs 3g, j).

Next, we discuss how the direct CO_2-forced HC response is amplified by climate responses mediated by sea surface warming. Contributions from eddy transport amplify the direct HC weakening in MLAT_DOM but are negligible in TROP_DOM (Eddy in Fig. 4c, e). In MLAT_DOM, the poleward eddy energy transport is substantially enhanced (Supplementary Fig. 3) associated with an increase in latent heat transport by transient eddies[33], indicating that less energy transport is required of the mean meridional circulation, thus resulting in HC weakening. Our results are consistent with Ref. [17], where the atmospheric eddy contribution is shown to play a central role in weakening the HC in CMIP models. Our experimental setup further informs that the extratropical CO_2 forcing is most responsible for driving the eddy-induced HC changes.

Contributions from gross moist stability partially offset the direct HC response to both TROP and MLAT forcings (GMS in Fig. 4c, e). The gross moist stability represents the HC energy transport efficiency per unit mass flux, which can be considered as the difference between upper- and lower-level moist static energy[34]. As the tropical troposphere follows a moist adiabat, increased CO_2 leads to a larger dry static energy increase in the upper than the lower troposphere, thus enhancing the gross moist stability. The robust rises in the tropopause and upward shift of the circulation result in a further increase of the gross moist stability via the potential energy component of moist static energy. Meanwhile, low-level moistening acts to reduce the gross moist stability[35], leading to a sizable cancellation between the different components of moist static energy. In TROP_DOM, the slight dominance of the dry static energy contribution leads to a modest increase in gross moist stability, acting to dampen the direct HC strengthening (Fig. 4c). In MLAT_DOM, the latent heat contribution outweighs the dry static energy contribution due to a substantial tropical surface warming[20] (Supplementary Fig. 1); this leads to a reduction in gross moist stability, dampening the direct HC weakening (Fig. 4e). As a result, when sea surface warming is inhibited, the HC strengthening due to gross moist stability changes is 73.1% reduced relative to GLOB_DOM (Supplementary Fig. 4). The gross moist stability decreases more in the southern than the northern tropics despite hemispherically symmetric forcing, which is associated with a greater low-level moisture increase due to the larger ocean fraction in the Southern Hemisphere. Hence, the HC strengthening arising from reduced gross moist stability for the southern cell is 2.3 times larger than that for the northern cell. This highlights the importance of the ocean fraction asymmetry in the northern and southern tropics in contributing to a hemispherically asymmetric HC intensity response.

Similarly, contributions from ocean heat uptake oppose the direct HC response (OHU in Fig. 4c, e). The ocean heat uptake responses (i.e., downward net surface heat flux anomalies) in the DOM experiments are shown in Fig. 5. The TROP forcing increases ocean heat uptake equatorward of 10°S/N due to intensified equatorial upwelling (Fig. 5c), accompanied by enhanced trade winds associated with the strengthened HC (see discussion in Ref. [20]). As a result, the dynamic ocean effect in TROP_DOM reduces the equator-to-pole atmospheric energy gradient, thus damping the direct HC intensification (Fig. 4c). Conversely, the MLAT forcing decreases the ocean heat uptake in the tropics while increasing it in the extratropics (Fig. 5e). The reduction in tropical ocean heat uptake is a result of weakened equatorial upwelling driven by the HC weakening[20]. Meanwhile, the increase in extratropical ocean heat uptake is associated with strong circumpolar upwelling in the Southern Ocean[36] and a slowdown of the Atlantic meridional overturning circulation[20,37] (Fig. 5f). As a result, the dynamic ocean effect in MLAT_DOM enhances the equator-to-pole atmospheric energy gradient, thus effectively dampening the direct HC weakening (Fig. 4e). As the opposing effect of ocean heat uptake is absent in the SOM configuration, the HC response is substantially amplified in SOM compared to DOM (compare 1st and 2nd columns of Fig. 3). In particular, the amplification is much more pronounced for the southern compared to the northern HC in response to MLAT forcing (Fig. 4e). This hemispheric asymmetry arises because a larger increase in ocean heat uptake takes place in the southern compared to the northern extratropics (Fig. 5e), potentially due to

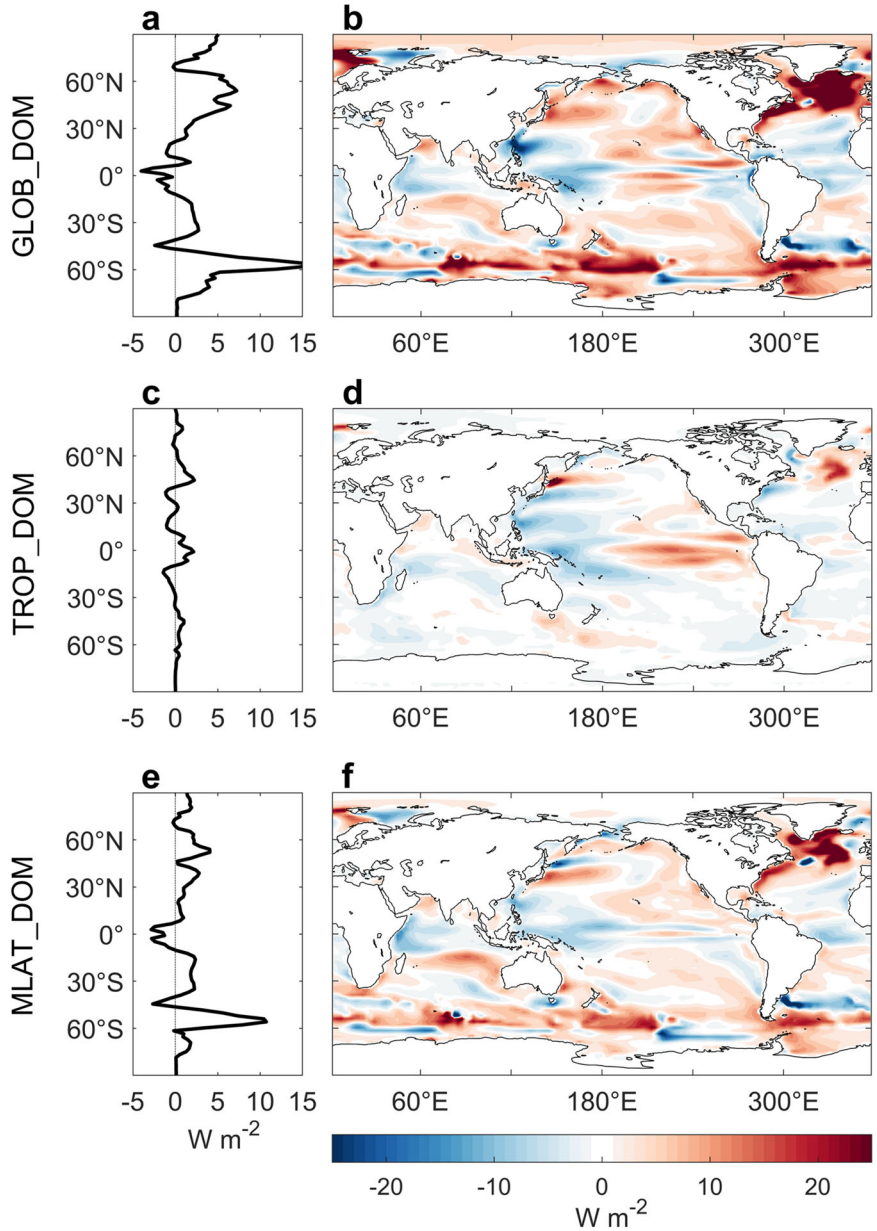

Fig. 5 Ocean heat uptake responses to CO_2 forcings. The annual- and zonal-mean ocean heat uptake responses (i.e., downward positive net surface heat flux) for **a** GLOB_DOM, **c** TROP_DOM, and **e** MLAT_DOM. **b**, **d**, **f** The spatial changes in ocean heat uptake corresponding to **a**, **c**, **e**.

a greater ocean fraction and continental geometry, so that the HC strengthening from ocean heat uptake is 4.8 times larger for the southern than the northern cell (Fig. 4e). A substantial southward shift of the HC in POLAR_SOM (Fig. 3n), responsible for the pronounced clockwise cross-equatorial HC response in GLOB_SOM (Fig. 3b), is caused by the strong positive feedback associated with Antarctic sea ice melt in the absence of a subpolar Southern Ocean damping effect (Fig. 5a, e).

Contributions of radiative feedbacks to the HC intensity changes

We now move to discuss how radiative feedbacks modulate the directly forced HC response. The effect of individual radiative feedbacks on the HC response, which is decomposed by Eq. (6) (see 'Methods'), is shown in the right column of Fig. 4. Briefly, the radiative kernel technique[38] and the APRP method[29] are combined to separate out the feedback contributions from changes in the temperature, water vapor, surface albedo, and clouds. A good match between SUM(Fdbk) and Fdbk in Fig. 4 indicates that individual contributions sum approximately to the actual radiative feedback contribution, which is defined by the difference between net TOA radiation response and radiative forcing (R_{Fdbk} in Eq. (6)), allowing for a linear decomposition of the radiative feedbacks. As the radiative feedbacks are reinforced by sea surface temperature changes, the feedback contribution is amplified in the DOM relative to FSST configuration (Supplementary Fig. 4).

Any feedback that decreases meridional atmospheric energy gradients contributes to a HC weakening. Thus, regardless of the forcing structure, the radiative feedbacks that are negative in the tropics and/or positive in the extratropics (e.g., temperature, surface albedo, shortwave cloud feedbacks; Fig. 6b, d, e) contribute to a HC weakening (Fig. 4). Note that the longwave emission is mediated by the responses in surface temperature (Planck feedback) and vertical profile of atmospheric temperature

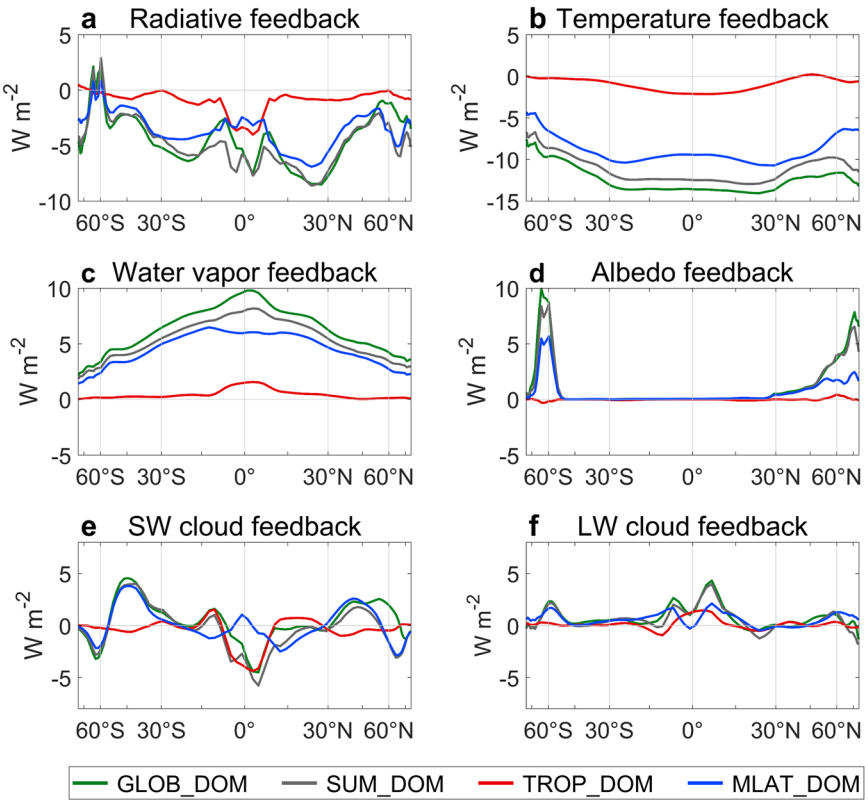

Fig. 6 Changes in radiative feedbacks in response to different CO_2 forcings. The annual- and zonal-mean profile of TOA radiation responses due to **a** total radiative feedback ΔR_{Fdbk}, **b** temperature feedback ΔR_T, **c** water vapor feedback ΔR_{WV}, **d** surface albedo feedback ΔR_A, **e** shortwave and **f** longwave component of the cloud feedback ΔR_C in GLOB_DOM (green), TROP_DOM (red), MLAT_DOM (blue), and the sum of all regional forcing experiments SUM_DOM (gray).

(lapse rate feedback), which are combined into the temperature feedback in this study. The meridional structure of the temperature feedback under global warming results in less poleward heat transport because the Planck feedback is more negative in the tropics while the lapse rate feedback is more positive in the polar region[39]. The reduction in the meridional energy gradient due to the temperature feedback is stronger in the Southern than Northern Hemisphere for MLAT forcing (Fig. 6b) associated with less surface warming in the extratropics due to a greater ocean heat uptake[40] (Supplementary Fig. 1), contributing to a larger HC weakening for the southern cell (T in Fig. 4f). The shortwave cloud feedback is negative in the tropics, primarily associated with enhanced deep convection in the warm pool region, whereas the extratropics for MLAT forcing exhibit a positive shortwave cloud feedback due to midlatitude cloud amount reduction[41] (Supplementary Fig. 5). The midlatitude positive shortwave cloud feedback in MLAT_DOM is particularly strong in the Southern Hemisphere (Fig. 6e) because of climatologically widespread marine boundary layer clouds associated with the larger ocean fraction[41], causing a preferential weakening of the southern cell (SWC in Fig. 4f).

In contrast, the meridional energy gradient is enhanced by the meridional structure of the water vapor feedback (Fig. 6c), contributing to a HC strengthening especially for MLAT forcing (WV in Fig. 4f) associated with a strong tropical warming and the Clausius-Clapeyron relationship[20] (Supplementary Fig. 1 and Supplementary Fig. 2). The longwave cloud feedback also strengthens the HC (LWC in Fig. 4) by amplifying the atmospheric energy content in the tropics (Fig. 6f) due to an increase in high-level clouds in the tropical warm pool region (Supplementary Fig. 5). However, the longwave component is overcompensated by the shortwave component, so that the net cloud feedback acts to weaken the HC (C in Fig. 4). We caution that our results are not necessarily representative of the HC impacts of cloud radiative feedbacks in other models because of large uncertainty in the shortwave cloud feedback[17,25,26,28] and emphasize the need for model intercomparison sensitivity studies to quantify this uncertainty.

The radiative feedbacks in sum weaken the HC in TROP_DOM by a comparable magnitude in the two hemispheres while strengthening the northern cell and weakening the southern cell in MLAT_DOM (SUM(Fdbk) in Fig. 4d, f). Despite a large hemispheric asymmetry in the radiative feedback contribution in MLAT_DOM, the total HC response shows a comparable weakening tendency in both hemispheres (STF in Fig. 4e). This is because large cancellation occurs in MLAT_DOM between a strong southern HC weakening from the radiative feedbacks and a strong southern HC strengthening from gross moist stability and ocean heat uptake, thereby leading to a weak hemispheric asymmetry in the total response.

DISCUSSION

In this study, we show that the HC intensity response under global warming is a result of compensating effects from regional CO_2 forcings by analyzing a series of hierarchical model experiments with idealized forcings in different latitude bands. We explain this compensation by decomposing the HC response in terms of contributions from radiative forcing, atmospheric eddies, gross moist stability, ocean heat uptake, and individual radiative feedbacks, as summarized in Fig. 7.

To first order, the HC response is determined by the latitudinal structure of the radiative forcing, with deep tropical CO_2 (TROP) forcing intensifying the HC and off-equatorial-to-midlatitude

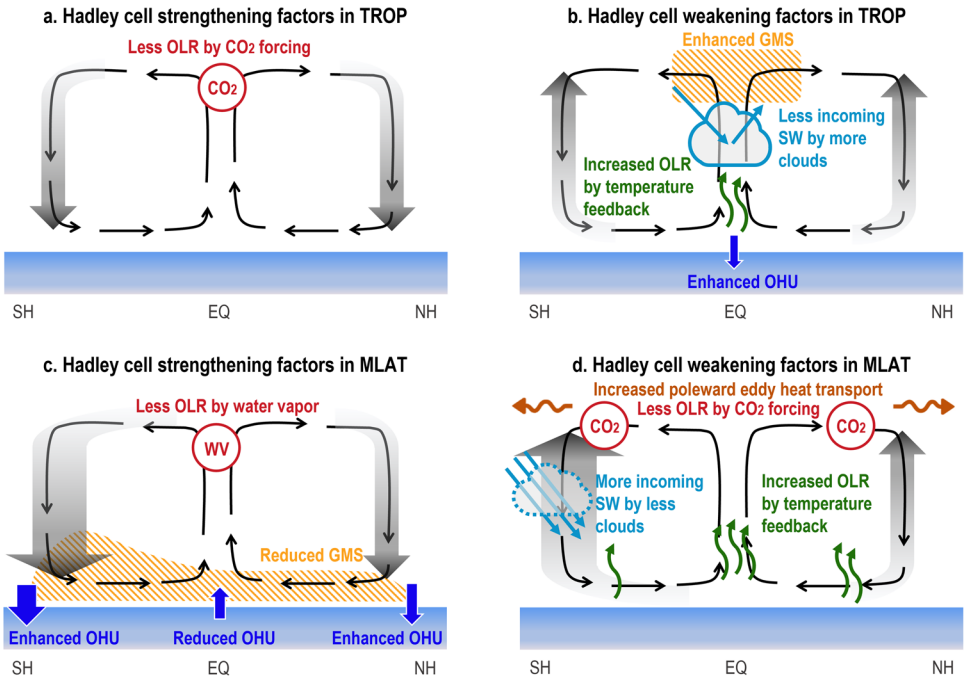

Fig. 7 Schematic summary of the physical processes explaining the distinct HC responses to different CO_2 forcings. a Main factor that causes HC strengthening in response to TROP forcing is the direct CO_2 forcing that enhances the meridional atmospheric energy gradient. **b** HC weakening in response to TROP forcing is caused by the temperature feedback, shortwave cloud feedback, enhanced gross moist stability, and enhanced heat uptake by the equatorial ocean. **c** HC strengthening in response to MLAT forcing is caused by the water vapor feedback, reduced gross moist stability, and increased ocean heat uptake by the extratropical oceans and decreased ocean heat uptake by the equatorial ocean. **d** HC weakening in response to the direct CO_2 forcing in MLAT is amplified by enhanced poleward eddy heat transport, shortwave cloud feedback, and temperature feedback.

(MLAT) forcing weakening the HC. While the competition between the regional radiative forcings is consistent with theoretical expectations[32], this hierarchy of experiments reveals a dominant role for mid-latitude forcing in provoking additional changes to the atmospheric energy budget that in turn affect the HC response. The direct CO_2-forced response is amplified by changes in atmospheric eddy energy transport, particularly for the MLAT_DOM in which poleward eddy heat transport substantially increases. Enhanced eddy energy transport implies reduced need for HC energy transport, thus weakening the HC. Meanwhile, the direct CO_2-forced response is damped by changes in gross moist stability and ocean heat uptake. For example, gross moist stability decreases in MLAT_DOM associated with low-level moistening, indicative of a less effective HC in transporting energy poleward, thereby contributing to a HC strengthening. The dampening effect by gross moist stability changes is also reported in Ref. [17]. Additional HC strengthening in MLAT_DOM is provided by a substantial increase in heat taken up by the extratropical oceans, due to strong circumpolar upwelling in the Southern Ocean and a slowdown of the Atlantic meridional overturning circulation, both of which enhance the meridional energy gradient. The role of ocean dynamics on dampening the HC weakening is consistent with Ref. [19].

Furthermore, individual radiative feedbacks modulate the HC strength by altering the meridional energy gradient. Any feedback that becomes more positive at lower latitudes enhances the meridional energy gradient, implying that the HC needs to transport more energy poleward, thus strengthening the HC, and vice versa. For example, the TOA radiation response due to water vapor feedback is more positive in the tropics than in the extratropics, contributing to a HC strengthening while the shortwave cloud feedback is negative in the tropics and positive in the extratropics, providing a HC weakening tendency, consistent with the results drawn from feedback locking experiments[27]. This consistency suggests that the APRP and radiative kernel technique can be used alternative to the feedback locking method to break down the circulation response into individual radiative feedback contributions.

Put together, the HC response is determined by intricate interactions among radiative forcing, radiative feedbacks, and ocean/atmospheric dynamical processes. While we emphasize the meridional gradient of the climate response, some studies highlight changes in the vertical temperature gradient as an important factor for determining the HC changes[31,40,42]. The effect of vertical distribution of temperature changes is represented by the gross moist stability in our framework. Although our results indicate that the gross moist stability change is not a key factor in CESM1, it could be crucial for explaining the inter-model spread, as argued by Ref. [31].

An important implication of this study is that the CO_2-induced HC changes fundamentally lack inter-model consistency not only because multiple factors affect the HC but also because regional radiative forcings impose opposing effects. We report a HC weakening contribution from MLAT forcing (i.e., CO_2 increase between 8°S/N–59°S/N) that is to a large degree compensated by a HC strengthening tendency from TROP forcing (i.e., CO_2 increase between 7°S–7°N) with a negligible contribution from POLAR forcing (i.e., CO_2 increase poleward of 60°S/N). While the negligible HC response to POLAR forcing is consistent with previous aquaplanet model results[22], the HC response to their TROP forcing (i.e., CO_2 increase between 20°S–20°N) contrasts with our results. A wider meridional extent of the TROP forcing region in Ref. [22] could be a cause for this inconsistency, so we examine the sensitivity to the forcing area by broadening the TROP forcing region to 15°S–15°N while narrowing the MLAT forcing region to 16°S/N–32°S/N using the experiment data from Ref. [20]. Consistent with our default experiment configurations, the HC responses to modified TROP and MLAT forcings are

opposite in sign (Fig. 3 vs Supplementary Fig. 6). That is, the compensating effect between the tropical and extratropical CO_2 forcing on the HC response is insensitive to the details of forcing structure in our model. The inconsistency with Ref. [22] suggests the need for a construction of a full model hierarchy ranging from an aquaplanet to a comprehensive DOM configuration. However, we note that our results are in line with another earlier idealized simulation of Ref. [21], which shows that the HC weakening response to an imposed tropical heating between 35°S–35°N becomes more pronounced with the thermal forcing between 20°S–20°N removed.

Thus, we argue that future HC intensity changes exhibit a considerable inter-model spread across the CMIP6 ensemble as a result of compensating effects from regional radiative forcings (Fig. 1b). Our results suggest that the HC response to regional forcings could be more robust because of the dominance of the direct radiative forcing contribution. We propose regional CO_2 forcing experiments as a useful benchmark helping to constrain the HC response to global CO_2 forcing and to reduce the uncertainty associated with individual feedbacks.

METHODS

Model experiments

We analyze a hierarchy of climate model experiments with prescribed latitudinally dependent CO_2 concentrations[23]. The model is the Community Earth System Model version 1.2.2 (CESM1.2.2)[30] with the finite volume Community Atmosphere Model version 4 (CAM4)[43]. The atmosphere and land models have a nominal 2° horizontal resolution, and the ocean and ice models have a nominal 1° horizontal resolution. The experiments are performed under three different model configurations: the atmospheric general circulation model fully coupled with a dynamic ocean model (DOM), thermodynamically coupled with a slab ocean model (SOM), and with fixed sea surface temperatures (FSST) as boundary conditions.

The DOM experiments, initialized from year 901 of a fully coupled pre-industrial control simulation, were perturbed by abruptly quadrupling the CO_2 concentration as a function of latitude (Fig. 2a) in the deep tropics (TROP; 7°S–7°N), the off-equatorial-to-midlatitudes (MLAT; 8°S–59°S and 8°N–59°N), the polar regions (POLAR; 60°S–90°S and 60°N–90°N), and the entire globe (GLOB; 90°S–90°N). Five ensemble members with small atmospheric initial condition differences were produced for the DOM perturbed experiments. All DOM experiments were integrated for 60 years and the ensemble-mean of the last 50-year average was used for the analysis. Note that 90% of the long-term mean responses (101–150 years) in the HC intensity occurs within the first 10 years in CO_2 quadrupling experiments[31], indicating that the 11–60 year response is reasonable for representing the long-term mean responses. The DOM control climate is a 50-year average of the pre-industrial simulation, from which the climatological monthly Q-flux was calculated for use in the SOM experiments. The SOM experiments were integrated for 120 years and the last 90 years were used for the analysis. The FSST experiments with SST and sea ice concentrations prescribed to the DOM control climatology were run for 80 years and the last 70 years were used for the analysis. The SOM and FSST experiments were perturbed in the same manner as the DOM experiments with the same CO_2 forcing structures.

Energetics constraint on the HC intensity

We attribute the fractional changes in HC intensity to the individual physical processes following Ref. [17]. In the annual-mean equilibrium state, the total atmospheric energy transport (F_a) can be determined by the zonal and meridional integral of net energy input to the atmospheric column:

$$F_a = \int_{-\frac{\pi}{2}}^{\phi}\int_0^{2\pi} (R_{toa} - Q_{net})' a^2 \cos\phi \, d\lambda \, d\phi, \quad (1)$$

where R_{toa} is the net radiative flux at TOA and Q_{net} is the downward positive net surface heat flux, representing the heat taken up by the ocean, which is the sum of ocean heat transport divergence and ocean heat storage. The prime denotes the deviations from the global mean, ϕ is latitude, λ is longitude, and a is the radius of the earth.

The mean component of F_a (denoted F_{HC}) can be directly calculated as the vertical integral of mean meridional moist energy flux:

$$F_{HC} = \frac{2\pi a \cos\phi}{g}\int_0^{p_s} [\overline{v}][\overline{h}]\, dp, \quad (2)$$

with the gravitational acceleration $g = 9.81$ m s^{-2}, the surface pressure p_s, the moist static energy $h = C_pT + gz + L_vq$, and the meridional velocity v. The time-mean and zonal-mean are indicated by an overbar and a bracket, respectively. Note that $[\overline{v}]$ is adjusted to be in mass balance, following Ref. [34].

In the tropics, the mean atmospheric energy transport F_{HC} can be expressed as

$$F_{HC} = \psi_{max} H, \quad (3)$$

where ψ_{max} denotes the HC mass flux, calculated as the maximum streamfunction $\psi(p,\phi) = \frac{2\pi a\cos\phi}{g}\int_0^p [\overline{v}]dp$ at each latitude, and $H \equiv F_{HC}/\psi_{max}$ denotes the gross moist stability, which measures the HC effectiveness in transporting energy poleward. Noting that $F_{HC} = F_a - F_e$ where the eddy component F_e is calculated as a residual. The fractional changes in mean energy transport for small perturbations (denoted by Δ) are given by

$$\frac{\Delta F_a - \Delta F_e}{F_{HC}} = \frac{\Delta\psi_{max}}{\psi_{max}} + \frac{\Delta H}{H}. \quad (4)$$

Substituting Eq. (1) into Eq. (4) gives

$$\frac{\Delta\psi_{max}}{\psi_{max}} = \frac{\int\int \Delta R'_{toa} - \int\int \Delta Q'_{net} - \Delta F_e}{F_{HC}} - \frac{\Delta H}{H}, \quad (5)$$

where the integrals are the same as in Eq. (1). Equation (5) indicates that the HC weakening may result from four factors: (1) reduced meridional gradients in the TOA radiation that decreases the need for the atmosphere to transport energy, (2) ocean heat uptake reduction in the extratropical oceans relative to the tropical oceans that decreases the meridional energy gradient, (3) enhanced eddy atmospheric energy transport that implies less energy gradient to be compensated by the HC, and (4) an increase in gross moist stability that implies more efficient HC in transporting energy poleward. The changes in R_{toa} in Eq. (5) can be further decomposed into the individual radiative feedbacks that represent the contributions from changes in the temperature, water vapor, surface albedo, and cloud feedback (see 'Decomposition of the TOA radiative flux changes' below).

Decomposition of the TOA radiative flux changes

We decompose ΔR_{toa} into the contributions of various radiative feedbacks and forcing:

$$\Delta R_{toa} = \Delta R_T + \Delta R_{WV} + \Delta R_A + \Delta R_C + \Delta R_f = \Delta R_{Fdbk} + \Delta R_f, \quad (6)$$

where ΔR_T, ΔR_{WV}, ΔR_A and ΔR_C are the radiative responses due to changes in the temperature, water vapor, surface albedo, and cloud feedback, respectively, and ΔR_f is the radiative forcing. The difference between ΔR_{toa} and ΔR_f defines the total feedback contribution ΔR_{Fdbk}. The longwave radiative responses are decomposed by the radiative kernel technique with specific humidity as the state variable for the water vapor feedback[38,44], while the shortwave component is decomposed by the approximate partial radiative perturbation (APRP) method[29]. The substitution of the APRP method for the shortwave component was employed because of substantial errors from monthly-mean shortwave radiative kernels[44–46]. Specifically, ΔR_T is estimated by the longwave temperature kernel, ΔR_{WV} by the combination of the moisture kernel (i.e., the longwave component of ΔR_{WV}) and the APRP non-cloud effect (i.e., the shortwave component of ΔR_{WV}), and ΔR_A by the APRP surface albedo effect. The cloud radiative response ΔR_C is calculated using the conventional radiative kernel technique for the longwave component and using the APRP method for the shortwave component. The radiative forcing ΔR_f is first estimated by the TOA longwave responses in the FSST experiments[47] and then corrected for the land surface temperature anomaly using the radiative kernels[48,49]. Without the correction for land surface warming, the forcing term erroneously includes radiative cooling from the Northern Hemispheric land area, artificially yielding hemispheric asymmetry in the direct radiative forcing contribution. Substituting Eq. (6) into Eq. (5) allows us to decompose the percentage changes in HC strength into the contributions from individual radiative feedbacks, radiative forcing, ocean heat uptake, eddy atmospheric energy transport, and gross moist stability. Compared to Ref. [17], we refine the decomposition method by applying

the APRP method and correcting for land surface warming in the forcing term. We note that these advances in the decomposition method are critical for reasonably decomposing the HC response in each hemisphere. These advanced techniques deserve attention for future radiative feedback analysis.

DATA AVAILABILITY

The post-processed model data for each figure are uploaded at https://doi.org/10.5281/zenodo.6365368. The CMIP data in Fig. 1 is available at https://esgf-node.llnl.gov/projects/esgf-llnl/.

CODE AVAILABILITY

MATLAB codes for the analysis of this study are available at https://doi.org/10.5281/zenodo.6365368.

Received: 26 March 2022; Accepted: 11 July 2022;
Published online: 01 August 2022

REFERENCES

1. Diaz, H. F. & Bradley, R. S. The Hadley Circulation: Present, Past and Future 1st edn, Vol. 1 (Springer, 2004).
2. Dai, A. Drought under global warming: A review. *WIREs Clim. Change* **2**, 45–65 (2011).
3. Post, D. A. et al. Decrease in southeastern Australian water availability linked to ongoing Hadley cell expansion. *Earths Future* **2**, 231–238 (2014).
4. Burls, N. J. et al. The Cape Town "Day Zero" drought and Hadley cell expansion. *Npj Clim. Atmos. Sci.* **2**, 27 (2019).
5. Rojas, M., Lambert, F., Ramirez-Villegas, J. & Challinor, A. J. Emergence of robust precipitation changes across crop production areas in the 21st century. *Proc. Natl. Acad. Sci.* **116**, 6673–6678 (2019).
6. Byrne, M. P. & Schneider, T. Narrowing of the ITCZ in a warming climate: Physical mechanisms. *Geophys. Res. Lett.* **43**, 11350–11357 (2016).
7. Huang, P., Xie, S.-P., Hu, K., Huang, G. & Huang, R. Patterns of the seasonal response of tropical rainfall to global warming. *Nat. Geosci.* **6**, 357–361 (2013).
8. Lau, W. K. M. & Kim, K.-M. Robust Hadley Circulation changes and increasing global dryness due to CO_2 warming from CMIP5 model projections. *Proc. Natl. Acad. Sci.* **112**, 3630–3635 (2015).
9. Su, H. et al. Weakening and strengthening structures in the Hadley Circulation change under global warming and implications for cloud response and climate sensitivity: Circulation, Clouds, Climate Sensitivity. *J. Geophys. Res. Atmos.* **119**, 5787–5805 (2014).
10. Kang, S. M. & Lu, J. Expansion of the Hadley cell under global warming: Winter versus summer. *J. Clim.* **25**, 8387–8393 (2012).
11. Lu, J., Vecchi, G. A. & Reichler, T. Expansion of the Hadley cell under global warming. *Geophys. Res. Lett.* **34**, L06805 (2007).
12. Scheff, J. & Frierson, D. M. W. Robust future precipitation declines in CMIP5 largely reflect the poleward expansion of model subtropical dry zones: POLEWARD EXPANSION OF CMIP5 DRY ZONES. *Geophys. Res. Lett.* **39**, L18704 (2012).
13. Vallis, G. K., Zurita-Gotor, P., Cairns, C. & Kidston, J. Response of the large-scale structure of the atmosphere to global warming. *Q. J. R. Meteorol. Soc.* **141**, 1479–1501 (2015).
14. Bony, S. et al. Robust direct effect of carbon dioxide on tropical circulation and regional precipitation. *Nat. Geosci.* **6**, 447–451 (2013).
15. Kang, S. M. Extratropical Influence on the Tropical Rainfall Distribution. *Curr. Clim. Change Rep.* **6**, 24–36 (2020).
16. Kang, S. M., Held, I. M., Frierson, D. M. W. & Zhao, M. The Response of the ITCZ to Extratropical Thermal Forcing: Idealized Slab-Ocean Experiments with a GCM. *J. Clim.* **21**, 3521–3532 (2008).
17. Feldl, N. & Bordoni, S. Characterizing the Hadley circulation response through regional climate feedbacks. *J. Clim.* **29**, 613–622 (2016).
18. Merlis, T. M. Direct weakening of tropical circulations from masked CO_2 radiative forcing. *Proc. Natl. Acad. Sci.* **112**, 13167–13171 (2015).
19. Chemke, R. & Polvani, L. M. Ocean Circulation Reduces the Hadley Cell Response to Increased Greenhouse Gases. *Geophys. Res. Lett.* **45**, 9197–9205 (2018).
20. Stuecker, M. F. et al. Strong remote control of future equatorial warming by off-equatorial forcing. *Nat. Clim. Change* **10**, 124–129 (2020).
21. Tandon, N. F., Gerber, E. P., Sobel, A. H. & Polvani, L. M. Understanding Hadley cell expansion versus contraction: Insights from simplified models and implications for recent observations. *J. Clim.* **26**, 4304–4321 (2013).
22. Shaw, T. A. & Tan, Z. Testing Latitudinally Dependent Explanations of the Circulation Response to Increased CO_2 Using Aquaplanet Models. *Geophys. Res. Lett.* **45**, 9861–9869 (2018).
23. Stuecker, M. F. et al. Polar amplification dominated by local forcing and feedbacks. *Nat. Clim. Change* **8**, 1076–1081 (2018).
24. Shaw, T. A. & Voigt, A. Land dominates the regional response to CO_2 direct radiative forcing. *Geophys. Res. Lett.* **43**, 11383–11391 (2016).
25. Ceppi, P. & Hartmann, D. L. Clouds and the Atmospheric Circulation Response to Warming. *J. Clim.* **29**, 783–799 (2016).
26. Ceppi, P. & Shepherd, T. G. Contributions of Climate Feedbacks to Changes in Atmospheric Circulation. *J. Clim.* **30**, 9097–9118 (2017).
27. Tan, Z. & Shaw, T. A. Quantifying the Impact of Wind and Surface Humidity-Induced Surface Heat Exchange on the Circulation Shift in Response to Increased CO_2. *Geophys. Res. Lett.* **47**, e2020GL088053 (2020).
28. Voigt, A. & Shaw, T. A. Circulation response to warming shaped by radiative changes of clouds and water vapour. *Nat. Geosci.* **8**, 102–106 (2015).
29. Taylor, K. E. et al. Estimating Shortwave Radiative Forcing and Response in Climate Models. *J. Clim.* **20**, 2530–2543 (2007).
30. Gent, P. R. et al. The Community Climate System Model Version 4. *J. Clim.* **24**, 4973–4991 (2011).
31. Chemke, R. & Polvani, L. M. Elucidating the Mechanisms Responsible for Hadley Cell Weakening Under 4 × CO_2 Forcing. *Geophys. Res. Lett.* **48**, e2020GL090348 (2021).
32. Held, I. M. & Hou, A. Y. Nonlinear Axially Symmetric Circulations in a Nearly Inviscid Atmosphere. *J. Atmos. Sci.* **37**, 515–533 (1980).
33. Wu, Y., Ting, M., Seager, R., Huang, H.-P. & Cane, M. A. Changes in storm tracks and energy transports in a warmer climate simulated by the GFDL CM2.1 model. *Clim. Dyn.* **37**, 53–72 (2011).
34. Hill, S. A., Ming, Y. & Held, I. M. Mechanisms of forced tropical meridional energy flux change. *J. Clim.* **28**, 1725–1742 (2015).
35. Chou, C., Wu, T.-C. & Tan, P.-H. Changes in gross moist stability in the tropics under global warming. *Clim. Dyn.* **41**, 2481–2496 (2013).
36. Armour, K. C., Marshall, J., Scott, J. R., Donohoe, A. & Newsom, E. R. Southern Ocean warming delayed by circumpolar upwelling and equatorward transport. *Nat. Geosci.* **9**, 549–554 (2016).
37. Marshall, J. et al. The ocean's role in the transient response of climate to abrupt greenhouse gas forcing. *Clim. Dyn.* **44**, 2287–2299 (2015).
38. Soden, B. J. et al. Quantifying Climate Feedbacks Using Radiative Kernels. *J. Clim.* **21**, 3504–3520 (2008).
39. Huang, Y., Xia, Y. & Tan, X. On the pattern of CO_2 radiative forcing and poleward energy transport. *J. Geophys. Res. Atmos.* **122**, 10578–10593 (2017).
40. Ma, J., Xie, S.-P. & Kosaka, Y. Mechanisms for tropical tropospheric circulation change in response to global warming. *J. Clim.* **25**, 2979–2994 (2012).
41. Frey, W. R. & Kay, J. E. The influence of extratropical cloud phase and amount feedbacks on climate sensitivity. *Clim. Dyn.* **50**, 3097–3116 (2018).
42. Son, S.-W., Kim, S.-Y. & Min, S.-K. Widening of the Hadley cell from last glacial maximum to future climate. *J. Clim.* **31**, 267–281 (2018).
43. Neale, R. B. et al. The Mean Climate of the Community Atmosphere Model (CAM4) in Forced SST and Fully Coupled Experiments. *J. Clim.* **26**, 5150–5168 (2013).
44. Shell, K. M., Kiehl, J. T. & Shields, C. A. Using the radiative kernel technique to calculate climate feedbacks in NCAR's community atmospheric model. *J. Clim.* **21**, 2269–2282 (2008).
45. Yoshimori, M., Hargreaves, J. C., Annan, J. D., Yokohata, T. & Abe-Ouchi, A. Dependency of feedbacks on forcing and climate state in physics parameter ensembles. *J. Clim.* **24**, 6440–6455 (2011).
46. Kim, H., Pendergrass, A. G. & Kang, S. M. The dependence of mean climate state on shortwave absorption by water vapor. *J. Clim.* **35**, 2189–2207 (2022).
47. Pincus, R., Forster, P. M. & Stevens, B. The Radiative Forcing Model Intercomparison Project (RFMIP): Experimental protocol for CMIP6. *Geosci. Model Dev.* **9**, 3447–3460 (2016).
48. Andrews, T. et al. Effective Radiative Forcing in a GCM With Fixed Surface Temperatures. *J. Geophys. Res. Atmos.* **126**, e2020JD033880 (2021).
49. Tang, T. et al. Comparison of Effective Radiative Forcing Calculations Using Multiple Methods, Drivers, and Models. *J. Geophys. Res. Atmos.* **124**, 4382–4394 (2019).

ACKNOWLEDGEMENTS

D.K., H.K., and S.M.K. are supported by the National Research Foundation of Korea (NRF) grant (NRF-2020R1A2C2101503) funded by the Ministry of Science and ICT (MSIT). M.F.S. was supported by NSF grant AGS-2141728 and NOAA's Climate Program Office's Modeling, Analysis, Predictions, and Projections (MAPP) program grant NA20OAR4310445. This is IPRC publication 1570 and SOEST contribution 11523.

AUTHOR CONTRIBUTIONS

M.F.S., S.M.K., and D.K. designed the study. M.F.S. conducted the model experiments. D.K. and H.K. analyzed the data and wrote the first draft. T.M.M. provided the theoretical background for the analysis. All co-authors contributed to the discussion of the results and writing of the manuscript. D.K. and H.K. contributed equally to this paper.

COMPETING INTERESTS

The authors declare no competing interests.

ADDITIONAL INFORMATION

Supplementary information The online version contains supplementary material available at https://doi.org/10.1038/s41612-022-00287-x.

Correspondence and requests for materials should be addressed to Sarah M. Kang.

Reprints and permission information is available at http://www.nature.com/reprints

Publisher's note Springer Nature remains neutral with regard to jurisdictional claims in published maps and institutional affiliations.